Novel Hierarchical Structure of MoS2/TiO2/Ti3C2Tx Composites for Dramatically Enhanced Electromagnetic Absorbing Properties

Heng Du
Zhengzhou University
Qipeng Zhang
Zhengzhou University
Biao Zhao
Zhengzhou Institute of Aeronautical Industry Management
Frank Marken
University of Bath
Qiancheng Gao
Zhengzhou Institute of Aeronautical Industry Management
Hongxia Lu
Zhengzhou University
Li Guan
Zhengzhou Institute of Aeronautical Industry Management
Hailong Wang
Zhengzhou University
Gang Shao
Zhengzhou University
Hongliang Xu
Zhengzhou University
Rui Zhang
Zhengzhou University
Bingbing Fan (fanbingbing@zzu.edu.cn)
Zhengzhou University https://orcid.org/0000-0002-1168-1142

Research Article

Keywords: MoS2/TiO2/Ti3C2Tx hierarchical hybrids, Microwave absorbing properties, dielectric loss

Posted Date: February 10th, 2021

DOI: https://doi.org/10.21203/rs.3.rs-184920/v1

Tel: 0086-371-67781590

E-mail: fanbingbing@zzu.edu.cn

Dr. Bingbing Fan

Zhengzhou University

NO. 100, Science Road, Zhengzhou, Henan 450001

P.R.China

Jan. 27, 2021

Dear editor,

We would like to submit the enclosed manuscript entitled **"Novel Hierarchical structure of $MoS_2/TiO_2/Ti_3C_2T_x$ Composites for Dramatically Enhanced Electromagnetic Absorbing Properties ",** which we wish to be considered for publication in ***Journal of Advanced Ceramics***. No conflict of interest exits in the submission of this manuscript, and manuscript is approved by all authors for publication. I would like to declare on behalf of my co-authors that the work described was original research that has not been published previously. It is not under consideration for publication anywhere; and publication has been approved by all co-authors and the responsible authorities at the institute(s) where the work has been carried out.

The novelty and significance of the work is as following:

(1) The $MoS_2/TiO_2/Ti_3C_2T_x$ hierarchical composites were prepared by one-pot hydrothermal method.

(2) Due to these hierarchical structures, the $MoS_2/TiO_2/Ti_3C_2T_x$ composites showed dramatically enhanced microwave absorbing performance.

(3) The effective absorption bandwidth covers 3.1 GHz (13.9–17 GHz) at the thickness of 1.0 mm, implying the features of wide frequency and light weight.

Suitable Referees:

1. Qing Yuchang, Northwestern Polytech Univ, State Key Lab Solidificat Proc, qtvbgyta@163.com, He is an expert in preparing microwave absorbing materials, he had reported the microwave absorbing properties of MXene in 2016.

2. Jin-SeoNoh, Gachon University Gachon Univ, Dept Phys, inseonoh@gachon.ac.kr, He is familiar with the Ti_3C_2 MXene and its composites.

3. Zhang Haobin, Beijing University of Chemical Technology, zhanghaobin@mail.buct.edu.cn, he is an expert in many kind of microwave absorbing materials, such as 2D materials, nanotube and so on.

We sincerely hope that you also find this manuscript worthy of consideration for ***Journal of Advanced Ceramics.*** If there is any problem please don't hesitate to inform us. We will try to modify it according to your suggestions. We are looking forward to hearing from you.

Thank you for your kind consideration.

Yours sincerely,

Bingbing Fan

Novel Hierarchical structure of $MoS_2/TiO_2/Ti_3C_2T_x$ Composites for Dramatically Enhanced Electromagnetic Absorbing Properties

Heng, Du[a, b, #], Qipeng Zhang[a, #], Biao Zhao[c], Frank Marken[d], Qiancheng Gao[c], Hongxia Lu[a], Li Guan[c], Hailong Wang, Gang Shao, Hongliang Xu, Rui Zhang[a, e], Bingbing Fan[a, *]

a. School of Materials Science and Engineering, Zhengzhou University, Zhengzhou 450001, China

b. The Key Laboratory of Functional Molecular Solids, Ministry of Education, Anhui Normal University, Wuhu, 241000, China

c. Henan Key Laboratory of Aeronautical Materials and Application Technology, Zhengzhou University of Aeronautics, Zhengzhou, 450046, China

d. Department of Chemtsiry, University of Bath, Claverton Down, BA2 7AY, Bath, UK

e. School of Materials Science and Engineering, Luoyang Institute of Science and Technology, Luoyang, 471023, China

#Heng, Du and Qipeng Zhang contribute equally to this work.

Corresponding Author: Bingbing Fan, fanbingbing@zzu.edu.cn

Abstract: In order to prevent the microwave leakage and mutual interference, more and more microwave absorbing devices are added into the design of electronic products to ensure its routine operation. In this work, we have successfully prepared $MoS_2/TiO_2/Ti_3C_2T_x$ hierarchical composites by one-pot hydrothermal method and focused on the relationship between structures and electromagnetic absorbing properties. Supported by comprehensive characterizations, MoS_2 nanosheets were proved to be anchored on the surface and interlayer of $Ti_3C_2T_x$ through a hydrothermal

process. Additionally, TiO_2 nanoparticles were obtained in situ. Due to these hierarchical structures, the $MoS_2/TiO_2/Ti_3C_2T_x$ composites showed greatly enhanced microwave absorbing performance. The $MoS_2/TiO_2/Ti_3C_2Tx$ composites exhibit a maximum reflection loss value of −33.5 dB at 10.24 GHz and the effective absorption bandwidth covers 3.1 GHz (13.9–17 GHz) at the thickness of 1.0 mm, implying the features of wide frequency and light weight. This work in the hierarchical structure $MoS_2/TiO_2/Ti_3C_2T_x$ composites opens a promising door to the exploration of constructing extraordinary electromagnetic wave absorbents.

Keywords: $MoS_2/TiO_2/Ti_3C_2T_x$ hierarchical hybrids, Microwave absorbing properties, dielectric loss

1. Introduction

Electronic products are developing towards the direction of high power and high frequency, but there is a major problem for these electronic products that they come with leakage and mutual interference of microwaves[1]. In order to resolve this problem, more and more electromagnetic wave absorbing devices are added into the design of electronic products to ensure routine operation. For practical microwave absorbing device applications, a new generation electromagnetic wave absorbers are expected to possess strong absorption capability and light weight, etc. To date, 2D nanomaterials such as graphene, graphene oxides (GOs)[2], MoS_2[3] and MXenes[4], have proven to be potential candidates for ideal microwave absorbers.

MXenes, an emerging group of layered materials, were synthesized by etching MAX phases by Gogotsi and co-workers in 2011[5]. They have a general formula of $M_{n+1}X_nT_x$, where M represents an early transition metal (*e.g.*, Ti, Mo, Nb, etc.), X usually is C and/or N, n = 1, 2, or 3, and T_x denotes surface terminations (=O, -OH, and/or -F). The distinguishing characteristics of MXenes, including special accordion-

like morphology, outstanding electrical conductivity, and rich functional groups surface, have captured enormous attention in many applications, especially for microwave absorption (MA)[6,7].

Since 2016, $Ti_3C_2T_x$ MXene has been developed as a potential microwave absorber candidate due to its positive dielectric loss ability[8]. Unfortunately, pure $Ti_3C_2T_x$ MXene alone is always limited to meet the requirement for practical application. Hence, incorporation of a second phase is very important. Semiconductors such as ZnO[9], SiC[10], MoS_2[11] and TiO_2[12] are usually introduced into $Ti_3C_2T_x$ to enhance microwave absorbing abilities due to their moderate dielectric constant, effective heterojunction formation and better impedance matching. Recently, a sandwich-like structure of the $MoS_2/TiO_2/Ti_3C_2Tx$ as nanocomposite was shown to possess improved microwave absorption ability when compared to the pure $Ti_3C_2T_x$[11]. However, the maximum reflection loss was just -16.0 dB, which is not satisfactory in practical applications.

The electromagnetic wave absorption properties of a material are closely related to the micro-structure[13]. Recent research in hierarchically structured materials opens a possible door into the exploration of constructing extraordinary electromagnetic wave absorbents[14]. So, in this work, we have successfully prepared $MoS_2/TiO_2/Ti_3C_2T_x$ hierarchical composites by one-pot hydrothermal method and focused on the relationship between structures and electromagnetic wave absorbing properties. Supported by comprehensive characterizations, MoS_2 nanosheets were proved to be anchored vertically on the surface and interlayer of $Ti_3C_2T_x$ through a hydrothermal process and in situ generated TiO_2 nanoparticles were obtained simultaneously. Due to these hierarchical structures, the $MoS_2/TiO_2/Ti_3C_2T_x$ composites showed greatly enhanced microwave absorbing performance.

2. Experimental

2.1. Chemicals

Ti_3AlC_2 raw powders were obtained from Institute of Metal Research, Chinese Academy of Sciences (with minimum purity: 99%, 200 mesh) and HF acid (40 wt%) was provided by Luoyang Chemical Reagent Factory. $Na_2MoO_4 \cdot 2H_2O$(with minimum purity: 99%) was purchased from Sinopharm Chemical Reagent Co., Ltd. CH_4N_2S (with minimum purity: 99%) was commercially obtained from Shanghai Aladdin Biochemical Technology Co., Ltd. Ethanol was supplied by Tianjin Fuyu Fine Chemical Co., Ltd. Deionized water (18.25MΩ·cm) was prepared by an ultra-pure water purifier (UPT-I-20L, ULUPURE).

2.2. Preparation of $Ti_3C_2T_x$

The $Ti_3C_2T_x$ nanosheets were prepared by a typical etching process of MAX phase Ti_3AlC_2[15]. 3.0 g Ti_3AlC_2 powder was added into 30 mL HF solution and stirred at room temperature for 12 h. Then, the $Ti_3C_2T_x$ suspension was centrifuged and washed by ethanol and deionized water several times until the pH value was above 6. The obtained precipitates were then freeze dried.

2.3. Preparation of $MoS_2/TiO_2/Ti_3C_2T_x$ composites

To synthesize $MoS_2/TiO_2/Ti_3C_2T_x$ composites, 0.1 g $Ti_3C_2T_x$ were dispersed in 70 mL deionized water. The solution was ultrasonicated for 5 min to form a uniform $Ti_3C_2T_x$ dispersion. After that, $Na_2MoO_4 \cdot 2H_2O$ and CH_4N_2S were dissolved into the $Ti_3C_2T_x$ suspension followed by stirring. The above solution was then transferred into a 100 ml Polyphenylene (PPL)-lined autoclave. The autoclave was kept at 200 °C for 12 h. After cooling naturally, the black precipitates were washed with deionized water and ethanol for many times. The samples were dried in a vacuum oven at 80 °C for 12 h. Based on the weight ratio of $Ti_3C_2T_x$ to MoS_2, i.e., 2:1, 1:1 and 1:2, the obtained

$MoS_2/TiO_2/Ti_3C_2T_x$ composites were labeled as S1, S2, and S3. For comparison, pure MoS_2 and $TiO_2/Ti_3C_2T_x$ powders were treated under the same procedure and condition. The schematic of the synthetic route and formation mechanism for the $MoS_2/TiO_2/Ti_3C_2T_x$ composites is depicted in Fig. 1.

2.4. Characterization

The morphology and microstructure of MoS_2, $TiO_2/Ti_3C_2T_x$ and $MoS_2/TiO_2/Ti_3C_2T_x$ composites were identified by field emission scanning electron microscopy (FESEM, JEOL JSM-7001F) and transmission electron microscopy (TEM, Jem-2100F). The crystal structure and phase composition were measured by X-ray diffractometer (XRD, Rigaku Ultima IV). Raman spectroscopy (HORIBA LabRAM HR Evolution, λ = 532 nm) was applied to determine the surface characteristics of the composites. X-ray Photoelectron Spectroscopy (XPS, ThermoFischer ESCALAB 250Xi) was employed to analyze the chemical states of the major elements on the sample surface.

2.5. Electromagnetic Measurements

For electromagnetic parameter measurements, S1, S2, S3 and MoS_2 powders were homogeneously dispersed in the paraffin wax with 60 wt%, respectively. All the above mixtures were pressed into toroidal-shaped (Outer Diameter = 7.00 mm and Inner Diameter = 3.04 mm). The relative complex permittivities of samples were measured using a vector network analyzer (Agilent, N5244A) in the frequency range of 2.0-18.0 GHz with the coaxial-line method.

3. **Results and discussion**

The typical XRD patterns of MoS_2, $TiO_2/Ti_3C_2T_x$ and $MoS_2/TiO_2/Ti_3C_2T_x$ composites are shown in Fig. 2 (a). The diffraction peak at 8.8 ° is considered to be a characteristic peak of $Ti_3C_2T_x$[3]. Compared with the pure $Ti_3C_2T_x$, there are two main diffraction peaks in $TiO_2/Ti_3C_2T_x$ composites at 25.6° and 27.4°, ascribed to anatase TiO_2 phase (JCPDS No. 21–1272) and rutile TiO_2 phase (JCPDS No. 83-2243), respectively[3]. It also could be seen that, after coupling with MoS_2, the relative peak intensity of TiO_2 is significantly weakened, while the diffraction peak intensity of $Ti_3C_2T_x$ is sharply enhanced, indicating that the formation of MoS_2 had inhibited the transformation process from $Ti_3C_2T_x$ to TiO_2. The characteristic diffraction peaks at 14.3 and 28.9 assigned to the (100) and (103) planes of MoS_2 (JCPDS card no. 37–1492)[16], while the peak of (002) plane of $Ti_3C_2T_x$ slightly shifts to 7.1°, demonstrating the d-spacing between $Ti_3C_2T_x$ nanosheets was expanded, and implying the successful anchoring of MoS_2 on the $Ti_3C_2T_x$ layers. The corresponding magnification of the range from 5-10° is shown in Fig. 2(b). It shows that the d-space of (002) plane of $Ti_3C_2T_x$ decreases with increase in MoS_2 content.

Raman spectroscopy of $TiO_2/Ti_3C_2T_x$ and $MoS_2/TiO_2/Ti_3C_2T_x$(S2) composites are shown in Fig. 3. The characteristic bands of $Ti_3C_2T_x$ at 261, 411, 606 cm^{-1} were observed[17]. In the spectrum of S2, the strong E_{2g}^1 mode at ~374 cm^{-1} corresponds to in-plane vibration and the A_{1g} mode at ~402 cm^{-1} is ascribed to the out-of-plane vibration. These are mainly due to the worse crystallinity of MoS_2, and due to the interaction between MoS_2 and $Ti_3C_2T_x$ nanosheets[18], which indicates that MoS_2 formed in the S2 samples. Additionally, the Ti-O peak appeared in all the samples. Compared with $Ti_3C_2T_x$, the Ti-O peak of both $TiO_2/Ti_3C_2T_x$ and $MoS_2/TiO_2/Ti_3C_2T_x$(S2) composites shifts to ~154 cm^{-1}, suggesting that more defects were generated during the hydrothermal process[19]. Furthermore, the strong D and G peaks of the composites are at 1382 and 1576 cm^{-1}, respectively. This illustrates that amorphous C was formed in the hydrothermal process[20].

Fig.4 (a) demonstrates that the bare MoS_2 spheres are composed of MoS_2 nanosheets. The average sphere diameter is about 12 μm. Fig.4 (b-d) exhibits FESEM images of $MoS_2/TiO_2/Ti_3C_2T_x$ composites. We observed that all the $MoS_2/TiO_2/Ti_3C_2T_x$ samples shared the same lamellar structure, indicating that the structure of $Ti_3C_2T_x$ is not destroyed during the hydrothermal process. The MoS_2 nanosheets are grown on the $Ti_3C_2T_x$ nanolayers, which could increase the specific surface area and expand the $Ti_3C_2T_x$ layer spacing. Moreover, as the MoS_2 content increased, the redundant MoS_2 nanosheets grown as nanospheres, anchored on the edge or entered into the $Ti_3C_2T_x$ inter-layers, as shown in Fig.4(d).

TEM and HRTEM were further applied to investigate the $MoS_2/TiO_2/Ti_3C_2T_x$ composites. As displayed in Fig. 5 (a), the $MoS_2/TiO_2/Ti_3C_2T_x$ composites are composed of Ti_3C_2 matrix and MoS_2 blanket with the average thickness around 80 nm. The interlayer spacing was considered to be about 0.61 nm, which matched the crystal planes of MoS_2 (002), as shown in Fig. 5 (b). These images further supported the hypothesis of the heterojunction structure of $MoS_2/TiO_2/Ti_3C_2T_x$ composites.

To confirm the surface properties of $MoS_2/TiO_2/Ti_3C_2T_x$ composites, S2 samples were analyzed by XPS. The survey spectra (Fig. 6a) and the high resolution XPS of Ti2p, C1s, O1s, Mo3d and S2p (Fig. 6b-f) are shown in Fig. 6. As shown in Fig. 6(a), we can see that the composites consist of Ti, C, O, Mo and S elements. In the Ti2p spectrum, The binding energies of the Ti-O $2p_{1/2}$ and $2p_{3/2}$ orbitals are 464.8 eV and 459.1 eV, and Ti-C $2p_{1/2}$ and $2p_{3/2}$ orbitals are 462.4 eV and 455.8 eV, respectively (Fig. 6b)[20]. In Fig. 6c, the C1s spectra can be separated into two peaks, related to C-C (284.7 eV) and C-O (285.9 eV), the weak peak at 281.8 eV is assigned to Ti-C bond[21]. The O1s profile was fitted by five symmetrical peaks. The fitting peak located at 530.3 eV

attributes to TiO_2. The peaks at 530.9, 531.7, 532.5, and 533.5 eV are assigned to C-Ti-Ox, C-Ti-(OH)x, Al_2O_3, and H_2O, respectively[22].

As for the Mo3d spectra in Fig. 6 (e), the obvious peaks located at 232.2, 229.0, and 226.1 eV are assigned to $Mo3d_{3/2}$, $Mo3d_{5/2}$, and S2s, respectively, confirming the Mo^{+4} ion exists in the nanocomposites[24]. There is an extremely small peak at 235.6 eV, which is correspond to the Mo (+6) $3d_{3/2}$ orbit, probably caused by the incompletely reduced MoO_4^{2-} during the hydrothermal procedure[23]. The S spectra of the $MoS_2/TiO_2/Ti_3C_2T_x$ composites can be divided into two peaks, and the peak at 163.2 eV and 161.9 eV corresponds to the S $2p_{3/2}$ and S $2p_{1/2}$, respectively.

Relative complex permittivity in the frequency range of 2-18 GHz was measured to clarify the electromagnetic wave absorbing property of the MoS_2 and MoS_2/Ti_3C_2Tx composites at room temperature. The real parts (ε') and the imaginary part (ε") represent the storage and the loss capability of electromagnetic energy[20]. As shown in Fig. 7(a) and (b), we can find that for the bare MoS_2, the ε' value is approximately 7.5 and almost kept constant with frequency, meanwhile, the ε" is within 1-2.3. After coupled with Ti_3C_2Tx, the complex permittivity is clearly enhanced, as the Ti_3C_2Tx content increased, the real part reaches to 13.8-34.5 and the imaginary parts fluctuates in the range of 2.1-12.9.

Higher complex permittivity demonstrates that the composites can store and dissipate much more electromagnetic energy, the real part of complex permittivity is an expression of interfacial and relaxation polarization mechanism [11]. For the MoS_2/Ti_3C_2Tx composites, higher ε' can be attributed to the improved interfacial and relaxation polarization effect arising from the multiple interfaces between the Ti_3C_2Tx and MoS_2 nanosheets.

Based on the theory of free electric, the imaginary part (ε") is related to the

conductivity, it can be illustrated as the following equation[25]:

$$\varepsilon'' = \sigma(2\pi f\varepsilon_0)^{-1}$$

Here σ, f and ε_0 represent the electrical conductivity, electromagnetic wave frequency and permittivity of free space, respectively. Consequently, higher conductivity brings higher ε" value. Owing to the excellent conductivity of Ti_3C_2Tx[26], the higher Ti_3C_2Tx content results higher conductivity of $MoS_2/TiO_2/Ti_3C_2T_x$ composites.

In addition, Fig. 7(c) shows the dependence of $\tan\delta_\varepsilon$ ($\tan\delta_\varepsilon = \varepsilon''/\varepsilon'$) on frequency of MoS_2 and $MoS_2/TiO_2/Ti_3C_2T_x$ composites, the $\tan\delta_\varepsilon$ values of $MoS_2/TiO_2/Ti_3C_2T_x$ composites exhibit a higher $\tan\delta_\varepsilon$ values than that of pure MoS_2, suggesting a superior dielectric loss ability of the $MoS_2/TiO_2/Ti_3C_2T_x$ composites. Due to the existence of the resonance phenomenon, the curve of S2 shows two distinct peaks.

According to the Debye's dipolar theory, the relationship of between ε' and ε" can be described as the following equation[27]:

$$(\varepsilon' - \frac{\varepsilon_s + \varepsilon_\infty}{2})^2 + (\varepsilon'')^2 = (\frac{\varepsilon_s + \varepsilon_\infty}{2})^2$$

Where ε_s stands for stationary frequency dielectric constant, and ε_∞ represents infinite frequency dielectric constant. As shown in Fig. 8. The Cole-Cole semicircles consist of several semicircles, which diverge from the ideal Cole-Cole semicircles, indicating the polarization and conductance loss mechanism in S2 samples. It is also well illustrated that both conduction loss and relaxation loss play important roles in dielectric loss.

The electromagnetic wave absorption performance of the MoS_2 and $MoS_2/TiO_2/Ti_3C_2T_x$ composites were investigated over 2-18 GHz and the reflection loss (R_L) are calculated by the following equations[12]:

$$R_L(dB) = 20\log\left|{(Z_{in} - Z_0)}\Big/{(Z_{in} + Z_0)}\right|$$

$$Z_{in} = Z_0\sqrt{\frac{\mu_r}{\varepsilon_r}}\tanh(j\frac{2\pi fd\sqrt{\mu_r\varepsilon_r}}{c})$$

Here f stands for the frequency of electromagnetic wave, d represents the thickness of the sample, c is the the velocity of EM wave, Z_{in} and Z_0 are the input impedance of the composite and free space, respectively, and ε_r and μ_r are the complex relative permittivity and complex permeability, respectively. In general, the R_L value exceeding -10 dB indicates 90% consumption of incident electromagnetic wave, implying an ideal electromagnetic wave absorber. As shown in Fig. 9(a), the maximum R_L of bare MoS_2 is -11.2 dB at 10.3 GHz with a thickness of 3.0 mm, suggesting its poor electromagnetic wave absorption properties. After coupling with $Ti_3C_2T_x$, the $MoS_2/TiO_2/Ti_3C_2T_x$ composites exhibit an enhanced electromagnetic wave absorption characteristic, the maximum R_L value of S1, S2 and S3 is -29.2 dB, -33.5 dB and -18.2 dB, respectively, as shown in Fig.9(b-d). Especially for S2, the effective absorption bandwidth (<10 dB) covers 3.1 GHz (13.9–17 GHz) at the thickness of 1.0 mm, implying the characteristic of wide frequency and light weight.

In general, the $MoS_2/TiO_2/Ti_3C_2T_x$ composites (S2) exhibited excellent electromagnetic wave absorption performance, which originated from three aspects: enhanced interface polarization relaxation, scattering effects and appropriate conductivity loss. The possible electromagnetic wave absorption mechanism of $MoS_2/TiO_2/Ti_3C_2T_x$ composites is proposed in Fig. 10. Firstly, the conductive laminate $Ti_3C_2T_x$ could enhance the conductance loss, and the unique laminated structure with MoS_2 as blanket could generate multiple reflections and scattering to attenuate electromagnetic waves. Furthermore, TiO_2 as a semiconductor, which could adjust the impedance matching properties, and the interface between MoS_2, TiO_2 and $Ti_3C_2T_x$ could also enhance the interface polarization effects.

4. Conclusion

$MoS_2/TiO_2/Ti_3C_2Tx$ composites were successfully prepared by a simple hydrothermal method. All the $MoS_2/TiO_2/Ti_3C_2T_x$ samples share the same lamellar structure, and the MoS_2 nanosheets are grown on the $Ti_3C_2T_x$ nanolayers, which could increase the specific surface area and expand the $Ti_3C_2T_x$ layer spacing. The $MoS_2/TiO_2/Ti_3C_2T_x$ composites exhibit a maximum reflection loss value of −33.5 dB at 10.24 GHz and the effective absorption bandwidth (<10 dB) covers 3.1 GHz (13.9–17 GHz) at the thickness of 1.0 mm, implying the features of strong absorption, wide frequency and light weight. The superior electromagnetic wave absorbing performance originated from the enhanced polarization relaxation, scattering effects and appropriate conductivity loss. This work in the hierarchical structure $MoS_2/TiO_2/Ti_3C_2T_x$ composites opens a promising door into the exploration of constructing extraordinary microwave absorbents.

Acknowledgment:

This work was financially supported by the National Natural Science Foundation of China (NO. U2004177), Outstanding Youth Fund of Henan Province (NO. 212300410081) and Natural Science Research Project of Henan Educational Committee (NO. 20A43001).

Reference:

1. Zhang F, Du H, Shang SY, *et al.* Constructing γ-MnO_2 Hollow Spheres with Tunable Microwave Absorption Properties. *Advanced Powder Technology* 2020, 31: 4642-4647.

2. Qin F, Brosseau C, Comment on “the Electromagnetic Property of Chemically Reduced Graphene Oxide and Its Application as Microwave Absorbing Material” [Appl. Phys. Lett. 98, 072906 (2011)]. *Applied Physics Letters* 2012, 100: 046101-046102.

3. Zhang XJ, Li S, Wang SW, *et al.* Self-Supported Construction of Three-Dimensional MoS_2 Hierarchical Nanospheres with Tunable High-Performance Microwave Absorption in Broadband. *The Journal of Physical Chemistry C* 2016, 120: 22019-22027.

4. Yao Y, Zhao J, Yang X. Recent Advance in Electromagnetic Shielding of Mxenes. *Chinese Chemical Letters* 2020, https://doi.org/10.1016/j.cclet.2020.07.029, In Press.

5. Naguib M, Kurtoglu M, Presser V, *et al.* Two-Dimensional Nanocrystals Produced by Exfoliation of Ti_3AlC_2. *Advanced Materials* 2011, 23: 4248-4253.

6. Jiang X, Kuklin AV, Baev A, *et al.* Two-Dimensional Mxenes: From Morphological to Optical, Electric, and Magnetic Properties and Applications. *Physics Reports* 2020, 848: 1-58.

7. Wang Z, Cheng Z, Fang C, *et al.* Recent Advances in Mxenes Composites for Electromagnetic Interference Shielding and Microwave Absorption. *Composites Part A: Applied Science and Manufacturing* 2020, 136: 105956-105973.

8. Qing Y, Zhou W, Luo F, *et al.* Titanium Carbide (Mxene) Nanosheets as Promising Microwave Absorbers. *Ceramics International* 2016, 42, 16412-16416.

9. Qian Y, Wei H, Dong J, *et al.* Fabrication of Urchin-Like Zno-Mxene Nanocomposites for High-Performance Electromagnetic Absorption. *Ceramics International* 2017, 43: 10757-10762.

10. Li X, Yin X, Xu, H, *et al.* Ultralight Mxene-Coated, Interconnected Sicnws Three-Dimensional Lamellar Foams for Efficient Microwave Absorption in the X-Band.

ACS Applied Materials & Interfaces 2018, 10: 34524-34533.

11. Wang H, Ma H. The Electromagnetic and Microwave Absorbing Properties of MoS_2 Modified Ti_3C_2Tx Nanocomposites. *Journal of Materials Science: Materials in Electronics* 2019, 30: 15250-15256.

12. Fan BB, Shang SY, Dai BZ, *et al.* 2D-Layered Ti_3C_2/TiO_2 Hybrids Derived from Ti_3C_2 Mxenes for Enhanced Electromagnetic Wave Absorption. *Ceramics International* 2020, 46: 17085-17092.

13. Zhang W, Zhang X, Wu H, *et al.* Impact of Morphology and Dielectric Property on the Microwave Absorbing Performance of MoS_2-Based Materials. *Journal of Alloys and Compounds* 2018, 751: 34-42.

14. Cui Y, Yang K, Wang J, *et al.* Preparation of Pleated rGO/MXene/Fe_3O_4 Microsphere and Its Absorption Properties for Electromagnetic Wave. *Carbon* 2021, 172: 1-14.

15. Shahzad F, Alhabeb M, Hatter CB, *et al.* Electromagnetic Interference Shielding with 2D Transition Metal Carbides (Mxenes). *Science* 2016, 353: 1137-1140.

16. Ning MQ, Lu MM, Li JB, *et al.* Two-Dimensional Nanosheets of MoS_2: A Promising Material with High Dielectric Properties and Microwave Absorption Performance. *Nanoscale* 2015, 7: 15734-15740.

17. Li JH, Rui BL, Wei WX, *et al.* Nanosheets Assembled Layered MoS_2/Mxene as High Performance Anode Materials for Potassium Ion Batteries. *Journal of Power Sources* 2020, 449: 227481-227287.

18. Zhang K, Ye M, Han A, *et al.* Characterization and Microwave Absorbing Properties of MoS_2 and MoS_2 -Reduced Graphene Oxide (rGO) Composites. *Journal of Solid State Chemistry* 2019, 277: 68-76.

19. Tran NM, Ta QTH, Noh JS. Unusual Synthesis of Safflower-Shaped TiO_2/Ti_3C_2 Heterostructures Initiated from Two-Dimensional Ti_3C_2 Mxene. *Applied Surface*

Science 2020, 538: 148023-148029.

20. Dai BZ, Zhao B, Xie X, *et al.* Novel Two-Dimensional $Ti_3C_2T_x$ Mxenes/Nano-Carbon Sphere Hybrids for High-Performance Microwave Absorption. *Journal of Materials Chemistry C* 2018, 6: 5690-5697.
21. Wang Y, Dou H, Wang J, *et al.* Three-Dimensional Porous Mxene/Layered Double Hydroxide Composite for High Performance Supercapacitors. *Journal of Power Sources* 2016, 327: 221-228.
22. Zheng M, Guo R, Liu Z, *et al.* MoS_2 Intercalated P-Ti_3C_2 Anode Materials with Sandwich-Like Three Dimensional Conductive Networks for Lithium-Ion Batteries. *Journal of Alloys and Compounds* 2018, 735: 1262-1270.
23. Mao ML, Mei L, Guo D, *et al.* High Electrochemical Performance Based on the TiO_2 Nanobelt@Few-Layered MoS_2 Structure for Lithium-Ion Batteries. *Nanoscale* 2014, 6: 12350-12353.
24. Jeong N, Kim HK, Kim WS, *et al.* Direct synthesis, characterization, and reverse electrodialysis applications of MoS_2 thin film on aluminum foil. *Materials Characterization*, 2020, 164: 110361-110368.
25. Ferrari AC. Raman Spectroscopy of Graphene and Graphite: Disorder, Electron-Phonon Coupling, Doping and Nonadiabatic Effects. *Solid State Communications* 2007, 143: 47-57.
26. Fan ZM, Wang DL, Yuan Y, *et al.* A Lightweight and Conductive Mxene/Graphene Hybrid Foam for Superior Electromagnetic Interference Shielding. *Chemical Engineering Journal* 2020, 381: 122696.
27. Li YP, Huang Y, Ding X, *et al.* $FeNi_3$ nanoalloy Decorated on 3D Architecture Composite of Reduced Graphene Oxide/Molybdenum Disulfide Giving Excellent Electromagnetic Wave Absorption Properties. *Journal of Alloys and Compounds* 2016, 689: 208-217.

Fig.1 The fabrication process of $MoS_2/TiO_2/Ti_3C_2T_x$ composites

Fig. 2 (a) XRD patterns of Ti_3C_2, MoS_2 and $MoS_2/TiO_2/Ti_3C_2T_x$ composites, (b) Magnification of XRD patterns in (a)

Fig.3 Raman spectroscopy of $TiO_2/Ti_3C_2T_x$ and $MoS_2/TiO_2/Ti_3C_2T_x$(S2) composites

Fig.4 FESEM images of MoS_2 (a) and $MoS_2/TiO_2/Ti_3C_2T_x$ composites (S2: b, S3: c and S4: d)

Fig.5 TEM(a) and HRTEM(b) images of $MoS_2/TiO_2/Ti_3C_2T_x$ composites (S2).

Fig.6 The survey spectra (a) and high resolution (b-f) XPS of $MoS_2/TiO_2/Ti_3C_2T_x$ composites (S2).

Fig.7 the electromagnetic parameters of MoS_2 and $MoS_2/TiO_2/Ti_3C_2T_x$ composites at 2-18GHz: (a) ε'; (b)ε''; (c) Dielectric loss tangent and (d) Attenuation constant.

Fig.8 Cole–Cole curves of $MoS_2/TiO_2/Ti_3C_2T_x$ composites (S2) samples

Fig.9 Reflection loss curves of MoS_2(a) and $MoS_2/TiO_2/Ti_3C_2T_x$ composites (b: S1; c: S2; d: S3) with different thickness.

Fig. 10 Diagrammatic drawing of the electromagnetic wave absorption mechanism of the $MoS_2/TiO_2/Ti_3C_2T_x$ composites

Figures

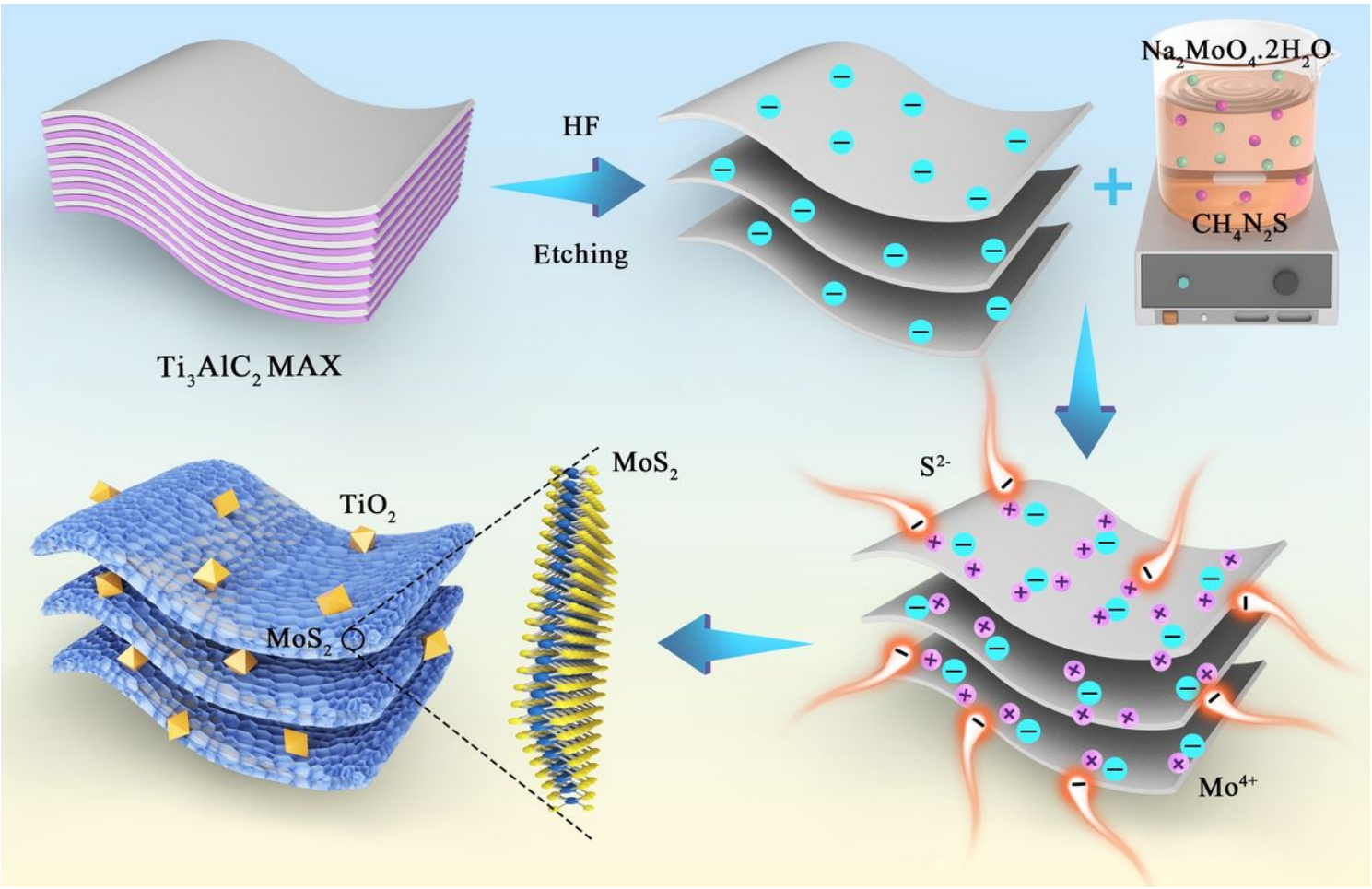

Figure 1

The fabrication process of MoS2/TiO2/Ti3C2Tx composites

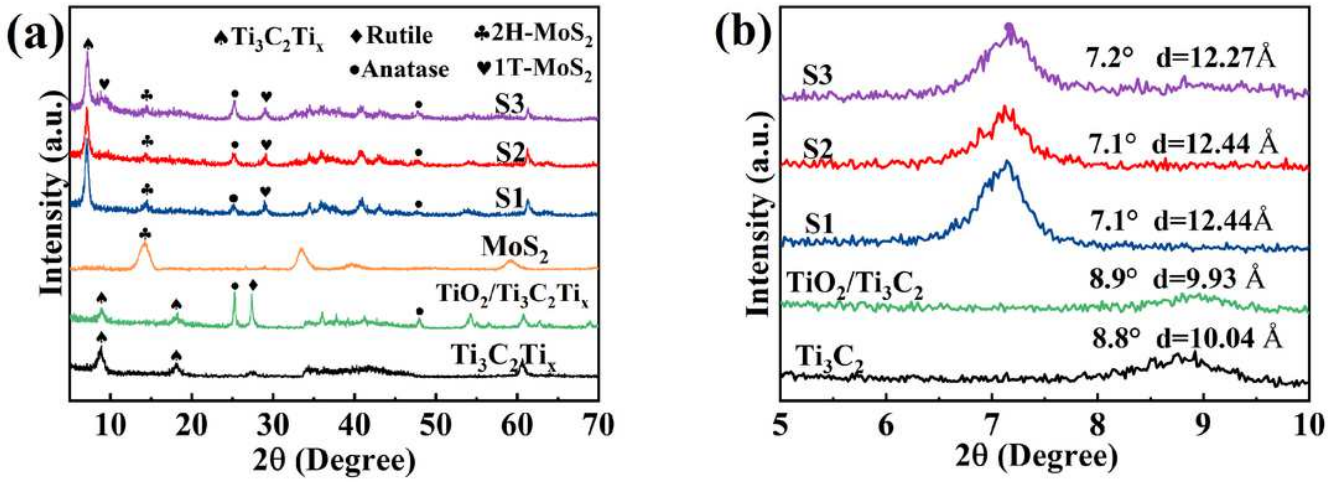

Figure 2

(a) XRD patterns of Ti3C2, MoS2 and MoS2/TiO2/Ti3C2Tx composites, (b) Magnification of XRD patterns in (a)

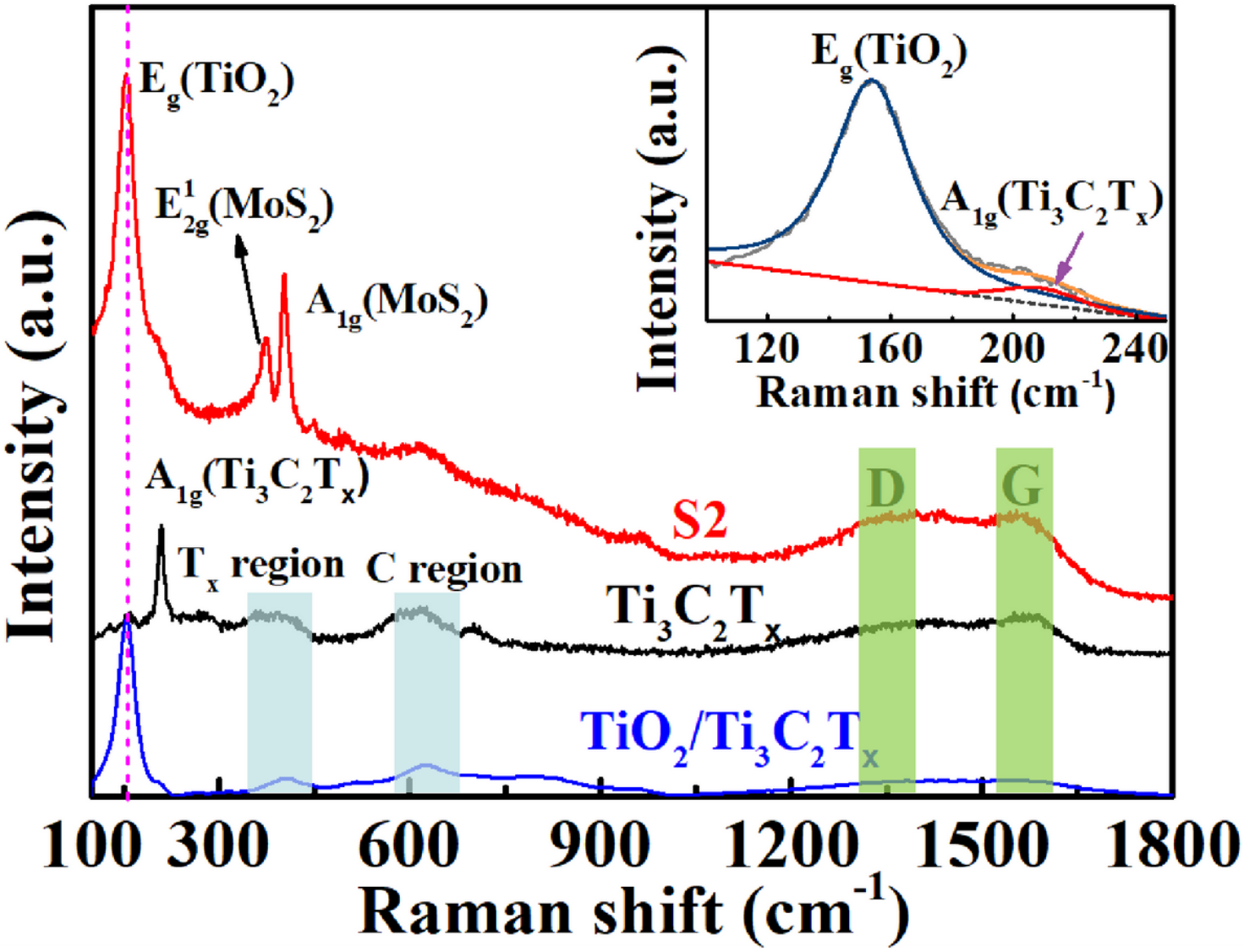

Figure 3

Raman spectroscopy of TiO2/Ti3C2Tx and MoS2/TiO2/Ti3C2Tx(S2) composites

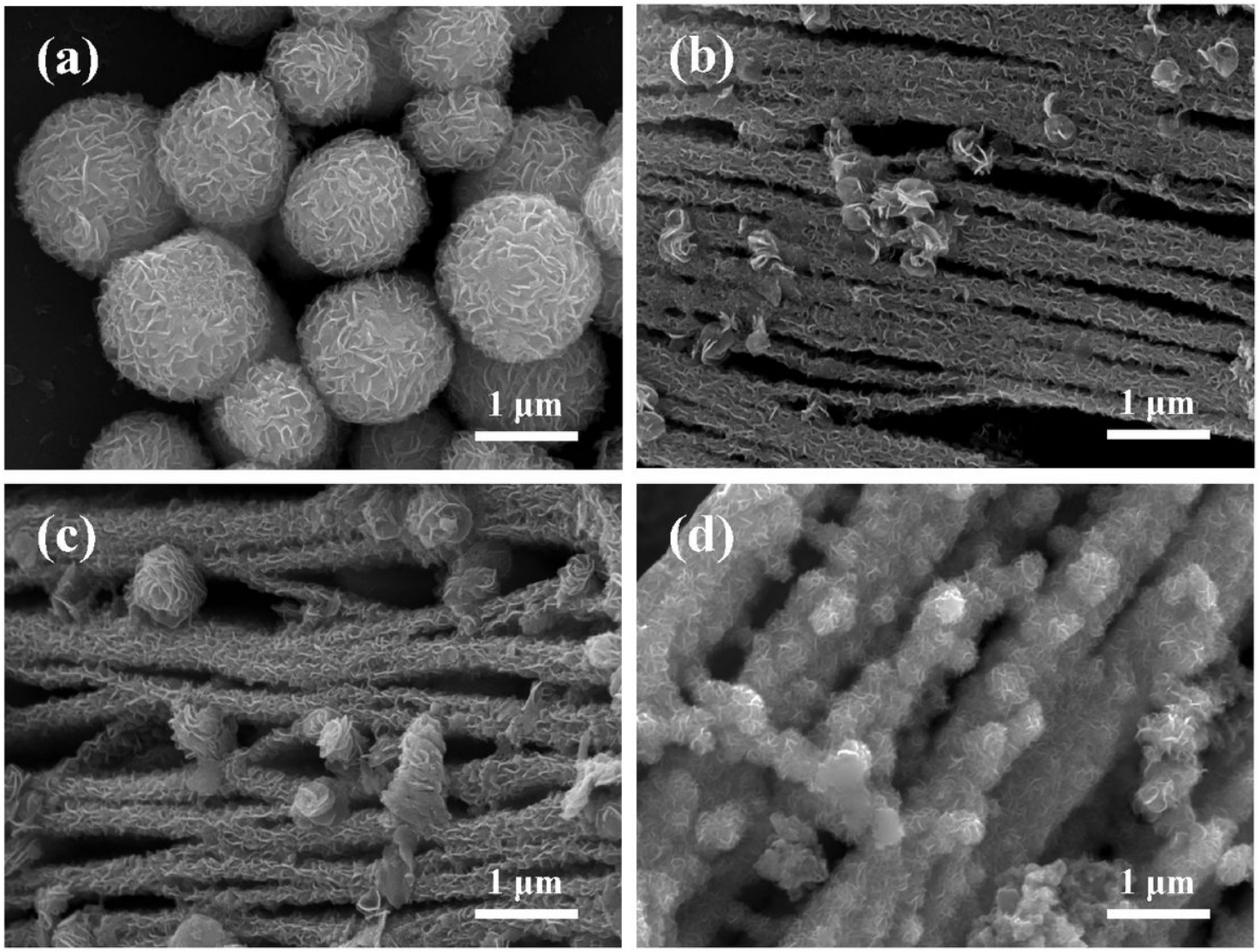

Figure 4

FESEM images of MoS2 (a) and MoS2/TiO2/Ti3C2Tx composites (S2: b, S3: c and S4: d)

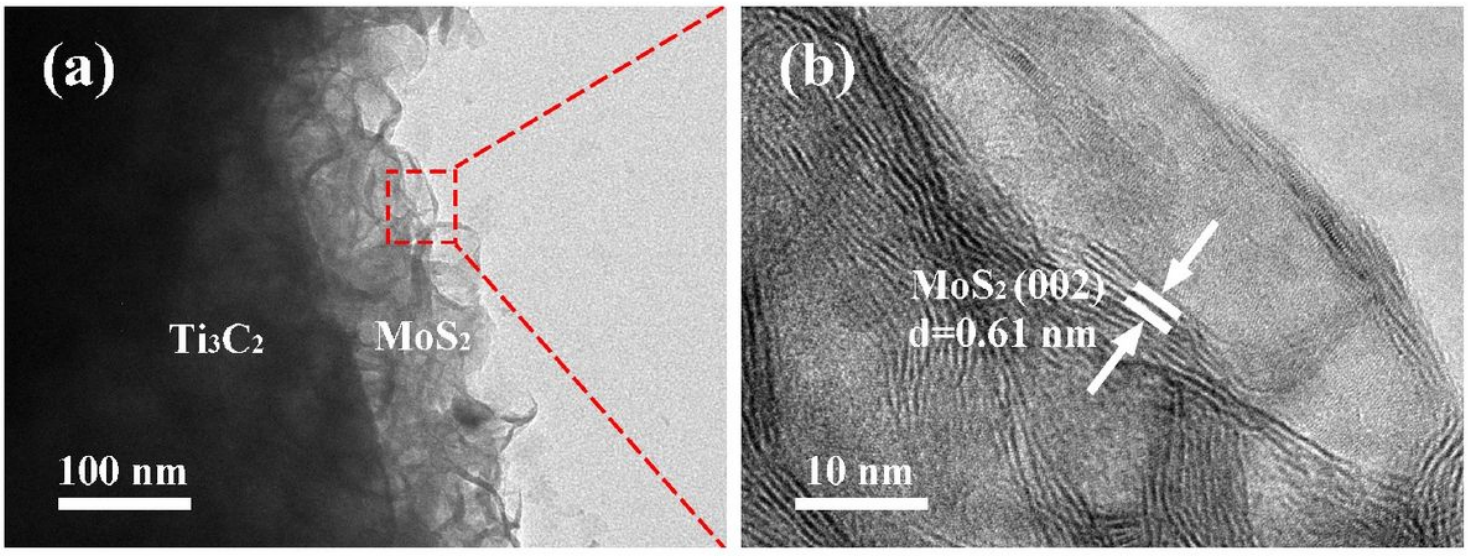

Figure 5

TEM(a) and HRTEM(b) images of MoS2/TiO2/Ti3C2Tx composites (S2).

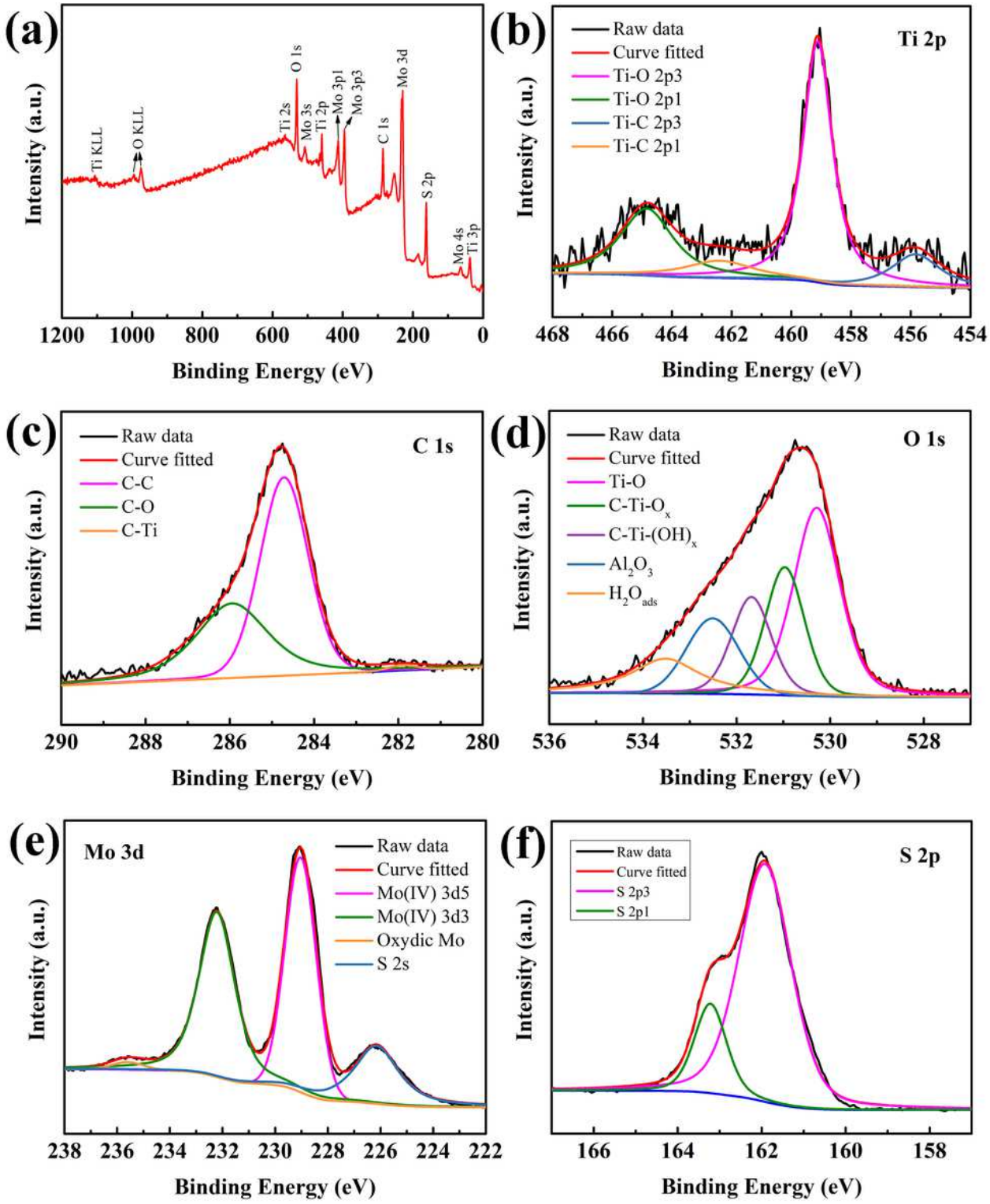

Figure 6

The survey spectra (a) and high resolution (b-f) XPS of MoS2/TiO2/Ti3C2Tx composites (S2).

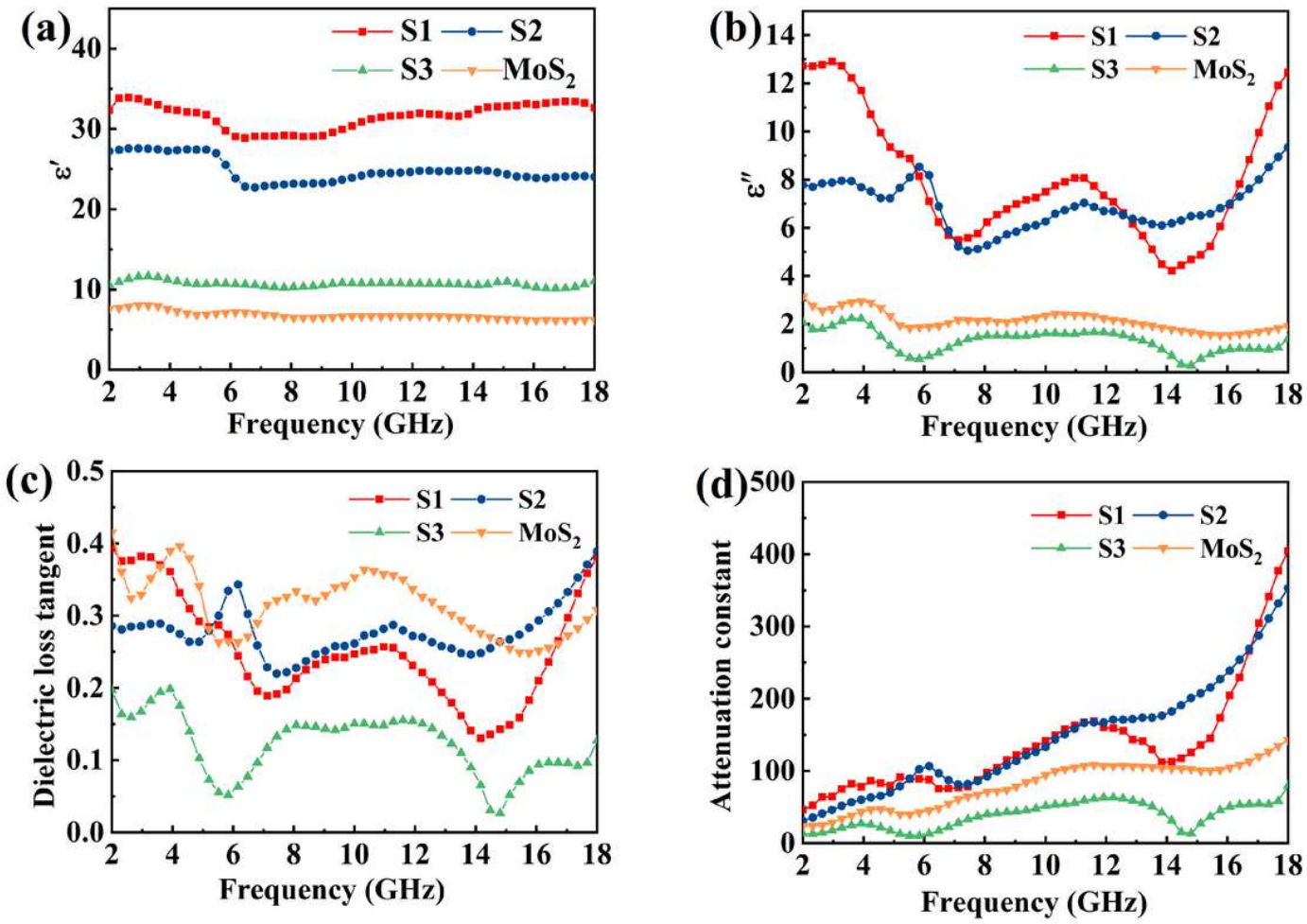

Figure 7

the electromagnetic parameters of MoS2 and MoS2/TiO2/Ti3C2Tx composites at 2-18GHz: (a) ε'; (b)ε"; (c) Dielectric loss tangent and (d) Attenuation constant.

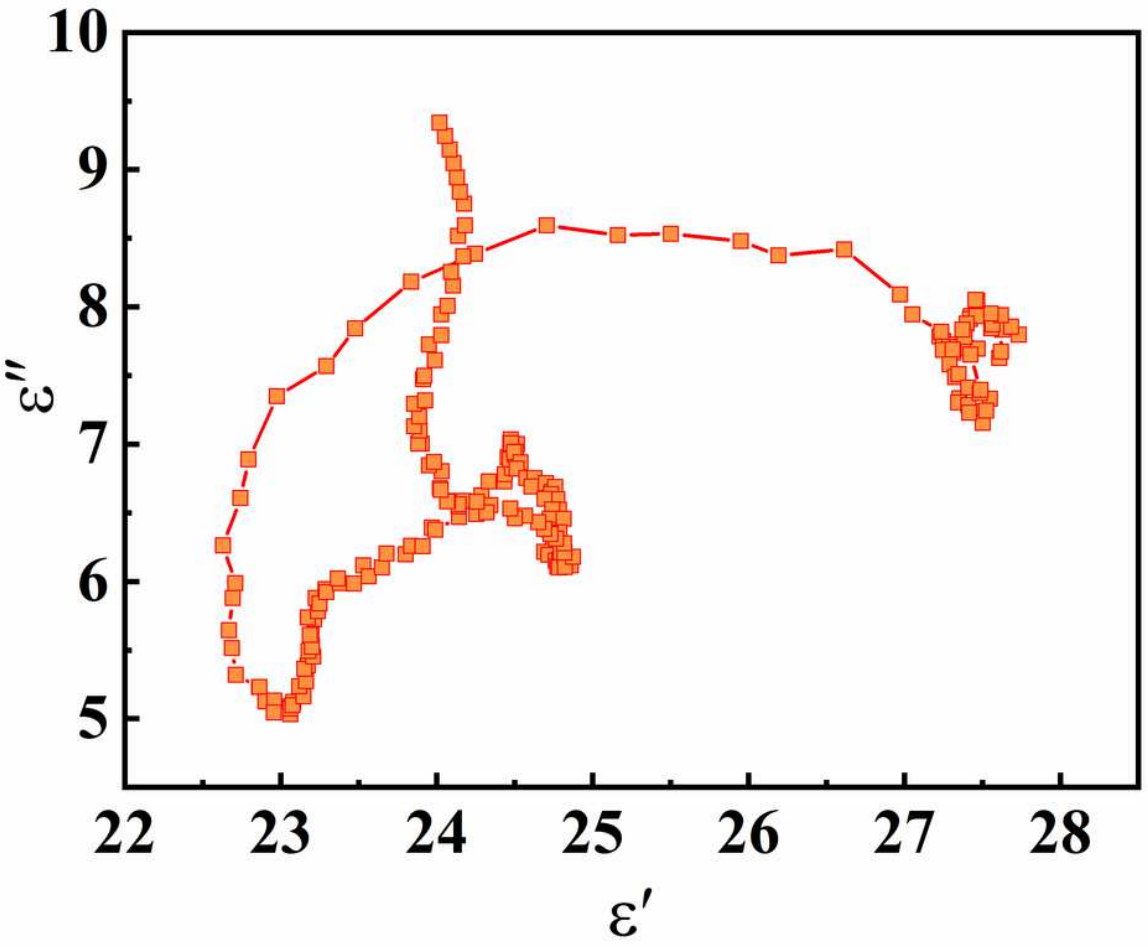

Figure 8

Cole–Cole curves of MoS2/TiO2/Ti3C2Tx composites (S2) samples

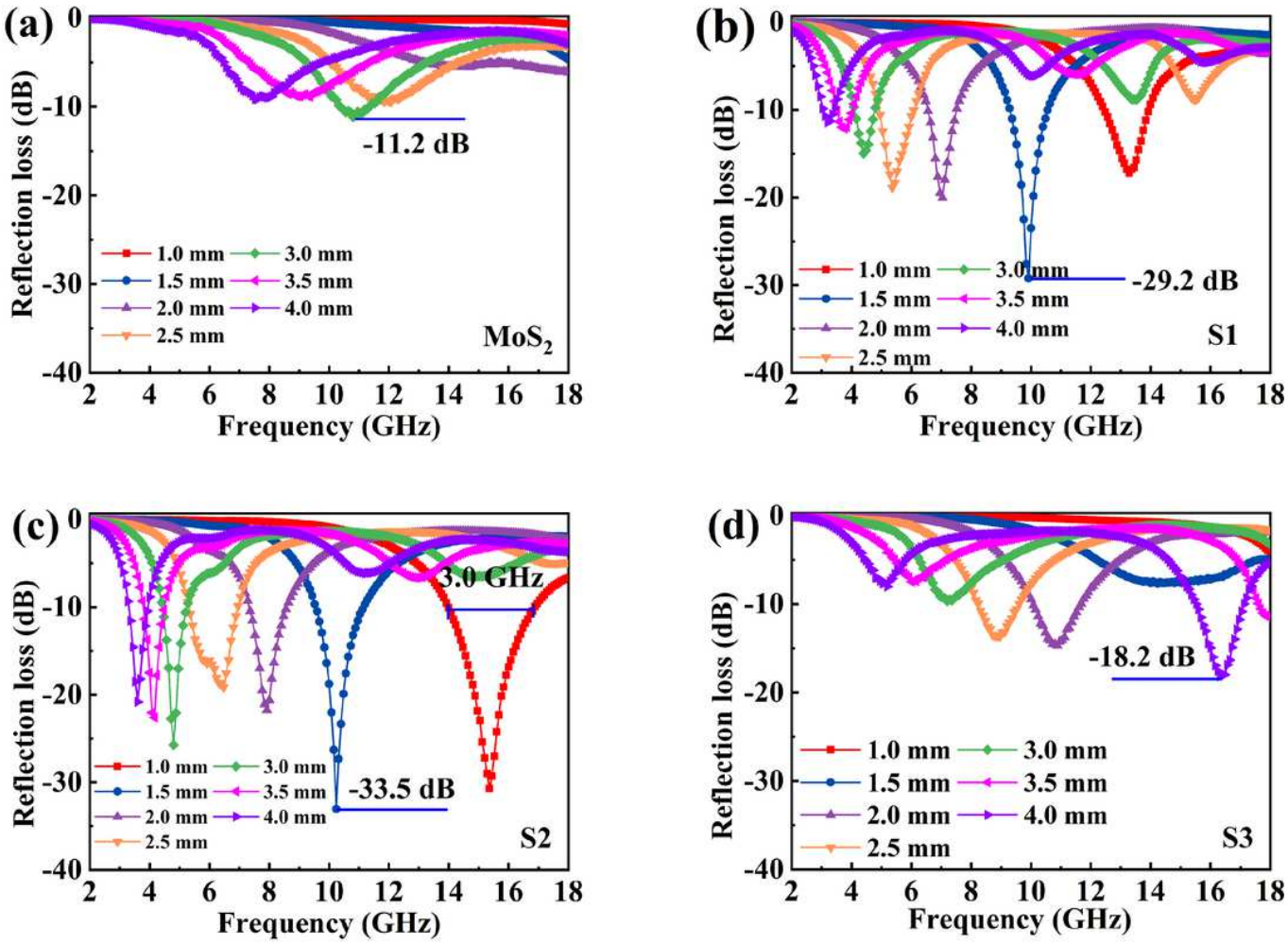

Figure 9

Reflection loss curves of MoS2(a) and MoS2/TiO2/Ti3C2Tx composites (b: S1; c: S2; d: S3) with different thickness.

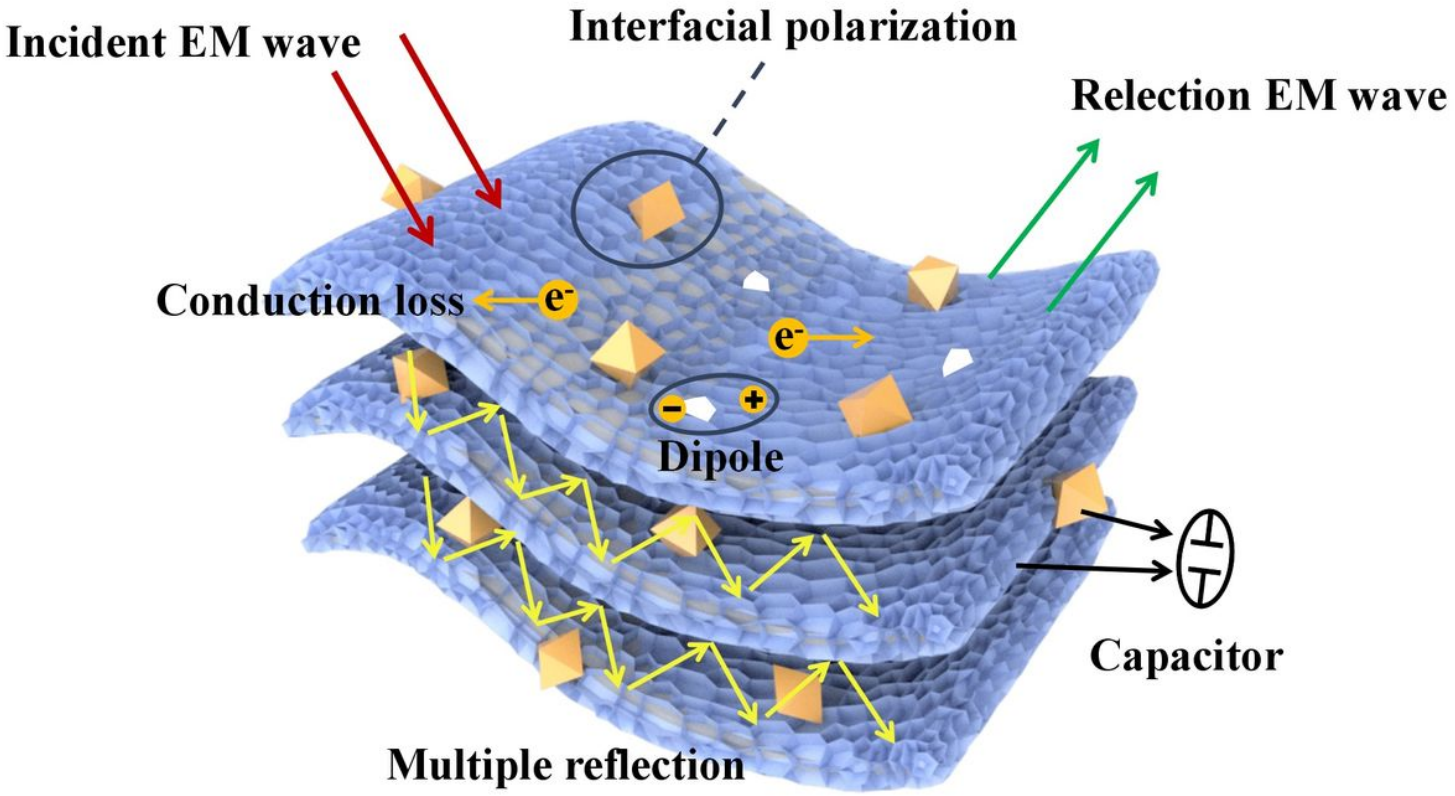

Figure 10

Diagrammatic drawing of the electromagnetic wave absorption mechanism of the MoS2/TiO2/Ti3C2Tx composites